Peeling, healing and bursting in a lubricated elastic sheet

A. E. Hosoi and L. Mahadevan

Peeling, healing and bursting in a lubricated elastic sheet

A. E. Hosoi[1, *] and L. Mahadevan[2, †]

[1]Hatsopoulos Microfluids Laboratory, Department of Mechanical Engineering,
Massachusetts Institute of Technology, 77 Massachusetts Avenue, Cambridge, MA 02139, USA
[2]Division of Engineering and Applied Sciences, Pierce Hall,
Harvard University, Cambridge, MA 02138, USA
(Dated: August 6, 2004)

We consider the dynamics of an elastic sheet lubricated by the flow of a thin layer of fluid that separates it from a rigid wall. By considering long wavelength deformations of the sheet, we derive an evolution equation for its motion, accounting for the effects of elastic bending, viscous lubrication and body forces. We then analyze various steady and unsteady problems for the sheet such as peeling, healing, levitating and bursting using a combination of numerical simulation and dimensional analysis. On the macro-scale, we corroborate our theory with a simple experiment, and on the micro-scale, we analyze an oscillatory valve that can transform a continuous stream of fluid into a series of discrete pulses.

We have all had the experience of the runaway transparency in the midst of a seminar; one that slides off the projector by riding on a thin film of air before coming to rest as far away from the speaker as possible [1]. The basic mechanism responsible for this event is the lubricating effect of a thin fluid film [2, 3]. This mundane situation is hardly unique and is indeed paradigmatic of many industrial processes such as the motion of magnetic tapes, paper in copying machines, and textile and polymeric film manufacturing [4]. On a much smaller scale, many biological and MEMS applications involving airway reopening in the lung [5], speech and song production in the vocal chambers [6], microfluidic pumps, valves and switches also involve the motion of flexible membranes close to walls [7, 8]. In all these situations, the moving flexible membrane is lubricated by the thin fluid film and responds by deforming; this deformation in turn changes the dynamics of the fluid film and thus leads to the competition between the elastic and fluid forces that eventually lead to the surly behavior of the unruly transparency. These problems are analogs of free-surface flows in hydrodynamics that arise in many applications (see [9] and references therein) but are qualitatively different owing to the presence of the elastic sheet. Nevertheless, the mathematical formulation of both classes of problems bears some similarities as we shall see.

An experimental realization of this class of problems is exemplified in Fig. 1. A flexible sheet of plastic is clamped at the left slightly above a rigid floor; when glycerine is pumped in from the lower left the plastic sheet lifts off and balloons as a peeling front advances to the right. Following a short transient, the front moves at constant velocity and the sheet eventually lifts off, completely supported by the fluid. In this letter, we will focus on some of the simplest problems motivated by this example, both on the macroscale and microscale using an asymptotic description of the "elastohydrodynamics" of fluid-lubricated elastic sheets.

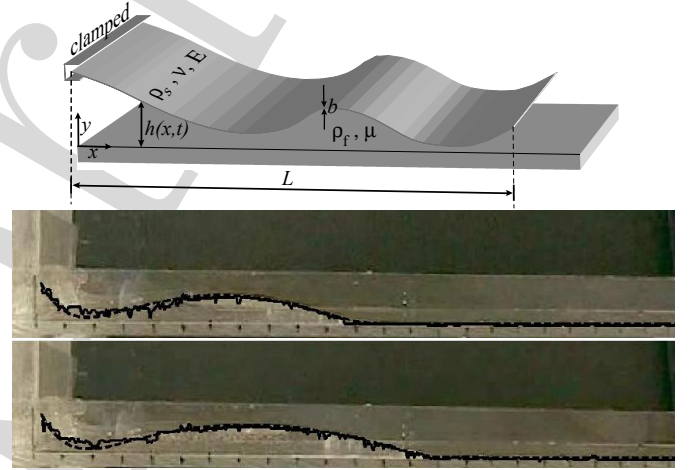We start by considering the two-dimensional dynam-

FIG. 1: A schematic of the system and images of a simple experiment showing a propagating peeling front in a plastic shim on a layer of glycerine. Dark solid lines indicate experimental data, dashed lines are the result of solving (7-8) numerically. These plots show two snapshots in time as the plastic peels off the underlying substrate. Experimental parameters are: $\rho_f = 1.2$ gm/cm^3, $\mu = 10$ gm/cm-s, $Q = 3.3$ cm^2/s, $E \approx 8.3 \times 10^{10}$ dynes/cm^2, $b \approx 0.1$ mm, $\Delta\rho = 5$ gm/cm^3. This corresponds to $H_g = 2.0$ cm, $L_g = 12.0$ cm and $\mathcal{G} = 283.2$.

ics of a fluid-lubricated elastic sheet of thickness b and length L ($L \gg H_g \gg b$ where H_g is a typical gap thickness), density ρ_s, Young's modulus E, Poisson ratio ν, and bending stiffness, $B = Eb^3/12(1-\nu^2)$ in a geometry shown shown in Fig. 1. The intercalating incompressible fluid of density ρ_f and viscosity μ satisfies the equations of momentum and mass conservation:

$$\rho_f(\mathbf{u}_t + \mathbf{u} \cdot \nabla\mathbf{u}) = -\nabla p + \mu\nabla^2\mathbf{u} + \rho_f\mathbf{g} \qquad (1)$$
$$\nabla \cdot \mathbf{u} = 0 \qquad (2)$$

where p is pressure, $\mathbf{u} = (u, v)$ is the fluid velocity, and $\mathbf{g} = (0, -g)$ is gravity. Along the rigid floor $y = 0$, the fluid does not slip or penetrate the solid so that $\mathbf{u}|_{y=0} = 0$ while along the elastic sheet $y = h(x,t)$, the no-slip con-

dition reads $u|_{y=h(x,t)} = 0$ and the kinematic boundary condition reads $h_t + u|_{y=h}h_x = v|_{y=h}$. Here and elsewhere subscripts denote derivatives. Finally, continuity of traction normal to the center line of the elastic sheet requires that

$$\mathbf{n} \cdot \sigma_f \cdot \mathbf{n} = \frac{Eb\,(1-\nu)}{(1+\nu)\,(1-2\nu)}\gamma h_{xx} - Bh_{xxxx}$$
$$- \rho_s b h_{tt} + f(h). \tag{3}$$

Here $\sigma_f = -p\mathbf{I} + \mu(\nabla\mathbf{u} + \nabla\mathbf{u}^T)$ is the fluid stress tensor, $\mathbf{t} = (1 + h_x^2)^{-1/2}(1, h_x), \mathbf{n} = (1 + h_x^2)^{-1/2}(-h_x, 1)$ are the tangent and outward normal to mid-plane of the elastic sheet, γ is the in-plane elastic strain and $\frac{Eb(1-\nu)}{(1+\nu)(1-2\nu)}\gamma h_{xx}$ is the contribution of the in-plane tension to out-of-plane forces, Bh_{xxxx} is the contribution due to out-of-plane bending, $\rho_s b h_{tt}$ is the inertia of the sheet, and $f(h)$ is a body force (per unit area) acting on the sheet. For the example shown in Fig. 1, $f(h) = -\Delta\rho g b = -(\rho_s - \rho_f)gb$ is the buoyancy-corrected weight of the sheet, while for the microscopic situation that we will treat later, $f(h) = \Pi(h)$ is the disjoining pressure due to van der Waals forces, although we note that gravity and van der Waals body forces will never appear together in physical situations. We have also assumed the sheet to be weakly tilted from the horizontal so that typical gap thicknesses are much smaller than characteristic bending length scales and $h_x \ll 1$. We quantify this by first noting that the horizontal length scale $L_g \equiv (Eb^3/|f(h_0)|)^{1/3}$ is set by the competition between bending and the external body force, and the vertical length scale $H_g = (\mu Q L_g/|f(h_0)|)^{1/3}$ is set by the competition between the external body force and viscous lift, where Q is the average flux in the gap. Furthermore the horizontal velocity scale is $U = Q/H_g$ while the vertical velocity scale is $V = \epsilon U$, where $\epsilon = H_g/L_g \ll 1$. Using these scales, we define the dimensionless variables $\hat{x} = x/L_g, \hat{y} = y/H_g = y/\epsilon L_g, \hat{u} = u/U, \hat{v} = v/\epsilon U, \hat{t} = Ut/L_g = L_g H_g t/Q, \hat{p} = p/P = p/f$. Substituting the scaled variables into (1-3), with $f = \Delta\rho g b$, we get (on dropping the hats)

$$\epsilon^2 Re(u_t + uu_x + vu_y) = -p_x + \epsilon^2 u_{xx} + u_{yy}$$
$$\epsilon^4 Re(v_t + uv_x + vv_y) = -p_y + \epsilon^4 v_{xx} + \epsilon^2 v_{yy} - \epsilon\mathcal{G},$$
$$u_x + v_y = 0 \tag{4}$$

subject to the boundary conditions $u|_{y=0} = u|_{y=h} = v|_{y=0} = 0, v|_{y=h} = h_t$, and

$$-p|_{y=h} + \left[\frac{2\epsilon^2}{1 + \epsilon^2 h_x^2}(v_y - h_x(u_y + \epsilon^2 v_x) + \epsilon^2 h_x^2 u_x)\right]_{y=h}$$
$$= \frac{(1-\nu)\,L_g H_g}{(1+\nu)\,(1-2\nu)\,b^2}\gamma h_{xx} - \frac{\epsilon h_{xxxx}}{12\,(1-\nu^2)}$$
$$-\epsilon^3 \frac{\rho_s Re}{\Delta\rho\mathcal{G}}h_{tt} + \frac{H_g^3}{\mu Q L_g}f(h). \tag{5}$$

Here $Re = \frac{QL_g\rho_f}{\mu H_g}$ is the Reynolds number and $\mathcal{G} \equiv \frac{\rho_f g H_g^3}{\mu Q}$ is the ratio of fluid hydrostatic pressure to viscous stresses. For an acetate sheet skimming over a table on a lubricating layer of air, the body force $f = -\Delta\rho g b$, $b \sim 10^{-2}$ cm, $E \sim 10^{10}$ dynes/cm^2, $\rho_s \sim 1$ g/cm^3, $\mu \sim 10^{-4}$ g/cm-s, $\rho_f \sim 10^{-3}$ g/cm^3, $U \sim 10$ cm/s so that $L_g \sim 10$ cm, $H_g \sim 0.3$ mm, $\mathcal{G} \sim 1$, $\epsilon \sim 10^{-3}$, $Re \sim 10^3$ (note that the scaled Reynolds number $\epsilon^2 Re \sim 10^{-3}$), thus both fluid and solid inertia are unimportant to leading order. In addition, provided the sheet has a free end and is sufficiently short [?], we can drop the γh_{xx} term in the normal stress boundary condition, further simplifying the analysis.

Using the fact that $\epsilon \ll 1$, we look for a solution to (4-5) of the form $u = u_0(x, y) + \epsilon u_1(x, y); v = v_0(x, y) + \epsilon v_1(x, y); p = p_o(x, y) + \epsilon p_1(x, y)$ etc. and find that, to order $O(\epsilon^2)$,

$$u \approx \frac{1}{2}p_x y\,(y - h),$$
$$p \approx \frac{H_g^3}{\mu Q L_g}f(h) + \epsilon\mathcal{G}\,(h - y) + \frac{\epsilon h_{xxxx}}{12(1-\nu^2)}. \tag{6}$$

Substituting these results into the depth-integrated continuity equation $h_t + (\int_0^h u\,dy)_x = 0$ yields a single nonlinear evolution equation for the transverse motion of the elastic sheet

$$h_t - \frac{\epsilon}{12}\left(\frac{h^3 h_{xxxxx}}{12(1-\nu^2)} + \mathcal{G}h^3 h_x + \frac{H_g^3}{\mu Q L_g}f_x\right)_x = 0 \tag{7}$$

This equation, valid in the limit of a thin fluid-filled gap, is similar to those seen in the context of free-surface flows [9] except for the term arising from elasticity, and represents a tremendous simplification from the PDEs that describe the coupled motion of the sheet and fluid. To complete the formulation of the problem, we need an initial profile and six boundary conditions. Motivated by the experiment shown in Fig. 1, for a clamped-free sheet, the appropriate boundary conditions are

$$\left.\begin{array}{l} h = h_0 \\ h_x = \theta_0 \\ q(h, h_x...) = 1 \end{array}\right\} \text{ at } x = 0 \quad \left.\begin{array}{l} h_{xx} = 0 \\ h_{xxx} = 0 \\ p = \frac{\epsilon\mathcal{G}}{2}h \end{array}\right\} \text{ at } x = L/L_g. \tag{8}$$

where $q(h, h_x...) = \int_0^h u\,dy$ is the fluid flux. The first three boundary conditions correspond to a prescribed height, slope and fluid flux at the clamped end $x = 0$, while the last three correspond to the condition of zero force, zero torque and a matched pressure at the free end.

For the peeling motion of a heavy macroscopic elastic sheet driven by a thin layer of viscous fluid shown in Fig. 1, $f = -\Delta\rho g b$. Solving the system (7-8) numerically using a finite difference method, we find that the numerical solution matches the experimentally observed transient peeling profiles (Fig. 1) with no adjustable parameters.
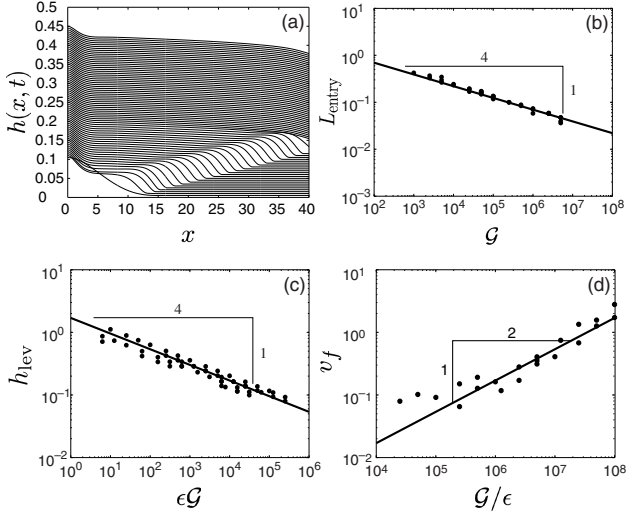
FIG. 2: (a) The evolution of a peeling front obtained by solving (7,8). Successive profiles are shifted vertically (thus time increases from bottom to top in the plot). (b) The entry length L_{entry} as a function of the dimensionless hydrostatic pressure $\mathcal{G}$; the line is the scaling law (9). (c) The levitation height h_{lev} as a function of $\epsilon\mathcal{G}$; the line is the scaling law (10). (d) The velocity of the peeling front v_f as a function of $\mathcal{G}/\epsilon$; the line is the scaling law (11). In each case, the points correspond to the results of numerical simulations of (7,8). In (d) Points deviate from the predicted scaling at small $\mathcal{G}$ where the assumption that hydrostatic effects dominate breaks down.

In Fig. 2(a) we show the evolution of the peeling traveling wave. Although these peeling waves are known to exist in the membrane-tension dominated regime [5], here they are dominated by bending and are thus qualitatively different. In the inlet region (roughly $x = 0$ to $x = 4$ in Fig. 2a) bending and hydrostatic forces balance each other so that $\frac{Eb^3\Delta H}{L_{\text{entry}}^4} \sim \rho g \Delta H$ which yields a scaling law for entrance length,

$$L_{\text{entry}} \sim L_g (\mathcal{G})^{-1/4}. \tag{9}$$

In the central region (roughly $x = 4$ to $x = 35$ in Fig. 2a), the membrane is relatively flat, and bending does not play a prominent role. The dominant balance is between viscous stresses and hydrostatic pressure so that $\frac{\rho_f g h_{\text{lev}}}{L_g} \sim \frac{\mu Q}{h_{\text{lev}}^3}$ leading to a scaling law for the levitation height

$$h_{\text{lev}} \sim H_g (\epsilon\mathcal{G})^{-1/4}. \tag{10}$$

The scaling laws (9, 10) are confirmed over a range of parameter values as shown in Fig. 2(b-c). Finally, in the outlet region, there is a small tail where the sheet is slightly curved to accommodate the free-end condition; the horizontal and vertical extent of this zone scale with L_g and H_g respectively, although there is a weak dependence on other parameters as well.

While these length scales characterize the steady levitating sheet, the transient behavior leading up to this

involves a peeling front moving at a velocity, v_f, which is constant as long as the front is sufficiently far from the inlet and the exit. At the front, the viscous power dissipated (per unit width) must be balanced by the work done against the hydrostatic load so that $\mu \left(\frac{v_f}{h_{\text{lev}}}\right)^2 h_{\text{lev}} L_g \sim \rho_f g L_g \left(L_p \frac{h_{\text{lev}}}{L_g}\right) v_f$. In dimensionless terms, this yields

$$\frac{v_f}{U} \sim \left(\frac{\mathcal{G}}{\epsilon}\right)^{1/2}. \tag{11}$$

This scaling law is confirmed numerically as shown in Fig. 2(d). As expected, the scaling breaks down for small $\mathcal{G}$ when hydrostatic forces no longer play a dominant role in the dynamics.

Having used this simple macroscopic setting as a test-bed for our theory, experiment and numerical simulations, we now turn to a micro-scale phenomenon motivated by fluid-actuated switches and valves in MEMS and microfluidics [7, 8], where van der Waals forces can potentially play a role. We consider the geometry shown in Fig. 1, but now set the body force to be the disjoining pressure between the elastic sheet and the rigid surface with $f = \Pi(h) = \frac{1}{6\pi}\left(\frac{A_r}{h^m} - \frac{A_a}{h^n}\right)$ in (3), where A_a and A_r are the attractive and repulsive Hamaker constants respectively; here $n = 3$ and $m = 9$ corresponding to the standard $(6, 12)$ Lennard-Jones potential. Following the asymptotic reduction procedure that led to (7) for the macroscopic problem now yields

$$h_t - \frac{\epsilon}{12}\left(\frac{h^3 h_{xxxxx}}{12(1-\nu^2)} + \mathcal{A}\frac{h_x}{h} - \mathcal{R}\frac{h_x}{h^7}\right)_x = 0 \tag{12}$$

where $\mathcal{A} = \frac{3}{6\pi}\frac{A_a}{\mu Q L_g}$ and $\mathcal{R} = \frac{9}{6\pi}\frac{A_r}{\mu Q L_g H_g^6}$ are rescaled Hamaker constants, with the length scales H_g, L_g defined using $f = \Pi(h_0)$ instead of $f = \Delta\rho g b$. Solving (12) subject to the boundary conditions (8), with $p|_{x=L/L_g} = \frac{H_g^3}{\mu Q L_g}\Pi(h)$, numerically we find two types of behavior. When repulsive effects dominate, the profile evolves to a steady state with gap thickness increasing monotonically in x. However, when repulsive and attractive effects are of the same order of magnitude, we observe time periodic bursting events as illustrated in Fig. 3(a). In this popping regime, the peeling and healing events are very asymmetric; peeling is relatively slow, while healing is extemely rapid. The peeling occurs with a roughly constant velocity when the front is sufficiently far away from the inlet/exit. When the front reaches the exit, the sheet bursts open releasing a small amount of fluid (Fig. 4a). The high pressure underneath the membrane is vented (Fig. 4b) and subsequently van der Waals forces cause the sheet to rapidly zip shut (Fig. 4c). This temporal asymmetry can be easily understood in terms of the characteristic gap thickness in the neighborhood of the propagating front. In the peeling case, fluid must be squeezed into a thin gap, slowing the front; in the healing
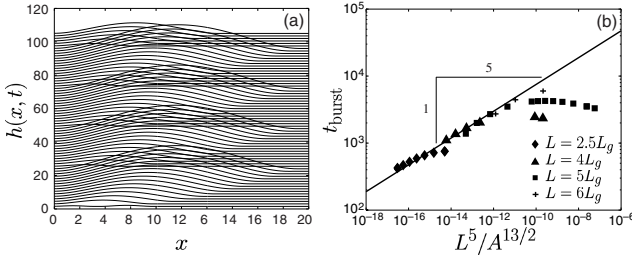
FIG. 3: (a) Bursting events driven by attractive van der Waals forces. As in Fig. 2(a), successive profiles are shifted vertically. $G = 0$, $\epsilon = 0.02$, $R = 0.1$, $A = 10^3$, and $H_g = 0.1$. (b) Scaling law for the time between bursting events t_{burst} when attractive van der Waals forces dominate. Points represent data from numerical simulations of (7,8); the line corresponds to the scaling law (13).

case, fluid may flow essentially unobstructed into the far reservoir.

Thus the amount of fluid released during each bursting event is dictated by the speed of the peeling front, v_p. To determine this, we note that the thickness of the smallest possible gap determined by the balance between attractive and repulsive van der Waals forces is given by $H_p \sim (\mathcal{R}/\mathcal{A})^{1/6}$, while a characteristic width of the peeling front L_p is set by balancing viscous and bending stresses, so that $\frac{\mu Q}{H_p^3} \sim \frac{Eb^3 H_p}{L_p^5}$ which yields $(L_p/L_g)^5 \sim \epsilon (H_p/H_g)^4$. Finally, at the front itself the power dissipated (per unit width) due to viscous effects must be balanced by the work done by the attractive van der Waals potential, so that $\mu \left(\frac{v_p}{H_p}\right)^2 H_p L_p \sim \frac{\mathcal{A}}{H_p^3}\left(L_p \frac{H_p}{L_p}\right) v_p$. Combining this with the condition that the time between bursting events t_{burst} is essentially a filling time, i.e. $t_{\text{burst}} v_p = L$ we find that $v_p/U \sim \mathcal{A}(H_g^9/\epsilon H_p^9)^{1/5}$ hence

$$t_{\text{burst}} \sim \left(\frac{L^5 n^5 \mathcal{R}^{3/2}}{\mathcal{A}^{5+3/2} H_g^8 L_g^6}\right)^{1/5}. \tag{13}$$

This scaling law is confirmed in Fig. 3(b) over a certain range of parameter values. However, the scaling law breaks down as $\mathcal{A}$ becomes small and the attractive forces become relatively weak. Choosing a typical value for the attractive Hamaker constant of $A_a \sim 10^{-13}$ dyne-cm, a flow rate of $U \sim 1$ cm/sec, $H_p \sim 100$ nm and $H_g \sim 100$ μm, gives a bursting time scale of $t_{\text{burst}} \sim 0.1$ sec suggesting that such a design might be experimentally feasible.

We conclude with a brief discussion of various generalizations of our ideas. Our main results are the evolution equations (7,12) that describes the motion of a wall-bounded elastic sheet or membrane in macroscopic and microscopic situations. Using these we study two simple phenomena, experimentally validate our theory and suggest how one might design an interesting microfluidic valve which acts like an inverter. A variety of other questions also lend themselves as natural candidates. These
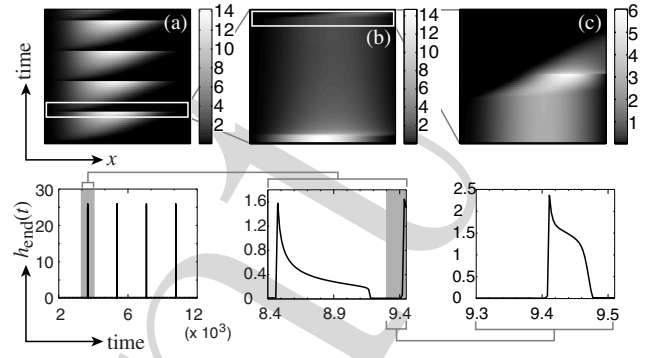

FIG. 4: (a) Top panel shows an alternative representation of the data in figure 3(a). Grey scale indicates gap thickness and time increases along the vertical axis. The sharp horizontal lines illustrate the rapid time scales associated with gap closure. The bottom panel shows the vertical position of the end of the membrane as a function of time. (b) Expanded view of the white box in (a) and associated time series for the vertical position of the end of the membrane illustrating venting. Time has been shifted by $t_{\text{shift}} = 2500$ to coincide with the first spike in (a). (c) Expanded view of the white box in (b) showing healing. Time has again been shifted by $t_{\text{shift}} = 2500$. The membrane zips shut from left to right expelling fluid.

include the free motion of a falling sheet of paper, which requires an additional equation for the horizontal velocity of the center of mass of the sheet, the touch-down of a sheet of paper (which admits a similarity solution), as well as generalizations to account for solid inertia to understand the flutter of the sheet in the context of voice and song production, all of which are subjects of current study.

---

* Electronic address: peko@mit.edu
† Electronic address: lm@deas.harvard.edu
[1] Benson, R.C. 1995. The Slippery sheet. *ASME J. Tribology*, **117**, 47.
[2] Tuck, E. O. and M. Bentwich. *J. Fluid Mech.*, **135**, 51-69 (1983).
[3] Reynolds O. *Philos. Trans. R. Soc., London, Ser. A*, **177**, 157 (1886).
[4] Gross, W., L. Matsch, V. Castelli, A. Eshel, J. Vohr, M. Wildmann. 1980. Fluid film lubrication. Wiley-Interscience, New York.
[5] Grotberg, J. B. and O. E. Jensen. *Ann. Rev. Fluid Mech.*, **36**, 121-147 (2004).
[6] Titze, I. 1994. Principles of voice production. Prentice Hall, New York.
[7] M. A. Unger, H-P Chou, T. Thorsen, A. Scherer and S. Quake. *Science*, **288**, 113 (2000).
[8] Whitesides, G. M. and A. D. Stroock. *Phys. Today*, **54**, 42 (2001).
[9] Oron, A., S. H. Davis and S. G. Bankoff. *Rev. Mod. Phys.*, **69**, 931 (1997).

[] The viscous shear stresses lead to a force of order $\mu U L / H_g$ and a stretching strain of order $\mu U L / H_g E b$. Comparing this with a typical bending strain $b H / L^2$ leads to a maximal length of the sheet $L \sim E b^2 H^2 / \mu U$ above which stretching effects cannot be ignored.